2006 IEEE International Conference on
Systems, Man, and Cybernetics
October 8-11, 2006, Taipei, Taiwan

Control Design for Vehicle's Lateral Dynamics

Der-Cheng Liaw and Wen-Ching Chung

***Abstract*—Issues of controllability and stabilization design for vehicle's lateral dynamics are presented. Based on the assumption of constant driving speed, a second-order nonlinear lateral dynamical model is obtained. It is observed that saddle node bifurcation will appear in vehicle dynamics with respect to the variation of the front wheel steering angle, which might result in spin and/or system instability. In order to possibly prevent the occurrence of such an instability, the controllability of vehicle dynamics at the saddle node bifurcation point is discussed. This leads to the design of a direct state feedback control law for system stabilization. Two-Parameter bifurcation analysis of system behavior is also obtained to classify the regime of the effective control gains for system stabilization. Numerical simulations for an example model demonstrate the effectiveness of analytical results.**

I. Introduction

Recently, the study of the vehicle's dynamics has attracted considerable attention [1]-[6]. One of the major goals of those studies is to enhance the driving safety since there have huge amount of traffic accidents occurring in daily life. It is known that those traffic accidents are highly related with the nonlinear behavior of vehicle dynamics. The linkage between the nonlinear phenomena of vehicle dynamics and the applied front wheel steering angle hence becomes a very important issue. Among those existing studies, sliding mode approach has been used to design robust control laws for providing system stability with respect to the large variation of system parameters such as axial velocity, mass of the vehicle and the contact force between tire and road surface [2]. A five degree-of-freedom vehicle model was used in [6] to design an extended Kalman filter (EKF) for estimating the historic data of vehicle's motion and corresponding tire forces. Based on a linear model of vehicle's lateral dynamics, linear control laws have been proposed in [3, 4]. Saddle-node bifurcation was observed in vehicle dynamics [5] to link with system instability via a numerical example. Such a bifurcation phenomenon might result in spin of the vehicle.

Bifurcation theory and its applications have been recently well exploited [7]-[11]. By applying the bifurcation theory, a theoretical analysis of vehicle dynamics has been obtained by Liaw et al [12], which revealed that the uncontrolled model of vehicle's lateral dynamics might undergo stationary saddle node bifurcation.

In this paper, we continue the study of vehicle's lateral dynamics as that in [12] but focus on the control issue. Here, we consider the nonlinear model of vehicle's lateral dynamics by assuming constant velocity in motion equations of steering dynamics without considering roll motion. In order to find the existence conditions of stabilization controller, system controllability at saddle node bifurcation point will be first discussed. Feedback control design will then be studied for preventing or delaying the appearance of saddle node bifurcation.

The paper is organized as follows. Mathematical models of vehicle system are recalled in Section II. It is followed by the analysis of existence and stability conditions for system equilibrium. The study of controllability at the saddle node bifurcation point and direct state feedback control design is given in Section IV. Finally, numerical studies for an example car model are given in Section V to demonstrate the analytical results.

II. Vehicle Dynamics

In the following, we recall the mathematical model for vehicle's steering dynamics from [1], which will be employed in the paper.

Consider the vehicle's steering dynamics as depicted in Fig. 1 (e.g., [1], [12]). Let both sideslip angle β and yaw rate γ be system outputs for the steering characteristics and the front-wheel angle δ_f be only system input. In addition, L_f denote the length between the center of gravity (CG) and front-wheel axes and L_r denote the length between CG and rear-wheel axes, respectively. Moreover, F_{yfl} and F_{yrl} (resp. F_{yfr} and F_{yrr}) are the left-side (resp. right-side) cornering force of front tires and rear tires, and both F_{xfl} and F_{xfr} (resp. F_{xfr} and F_{xrr}) are the left-side (resp. right-side) traction force of front and rear tires. For simplicity and without loss of generality, here, we assume the vehicle body is symmetric about the longitudinal plane. Let $F_{yf} = F_{yfl} + F_{yfr}$, $F_{yr} = F_{yrl} + F_{yrr}$, $F_{xf} = F_{xfl} + F_{xfr}$ and $F_{xr} = F_{xrl} + F_{xrr}$. The basic motion equations for steering dynamics with roll motion neglected was derived in [1] as given by

$$m(\dot{v} - v\beta r) = F_{xf} + F_{xr} - F_{yf}\sin\delta_f, \tag{1}$$

$$mv\cdot(\dot{\beta} + r) = F_{yf} + F_{yr} + F_{xf}\sin\delta_f, \tag{2}$$

$$I_z\dot{\gamma} = (L_f F_{yf} - L_r F_{yr})\cos\beta + L_f F_{xf}\sin\delta_f, \tag{3}$$

where

m : the mass of the vehicle,

I_z : the yaw moment around z-axis,

Manuscript received March 15, 2006. This work was supported in part by the Ministry of Education, Taiwan, R.O.C. under Grant EX-91-E-FA06-4-4.

Der-Cherng Liaw, Corresponding author, Professor, Department of Electrical and Control Engineering, National Chiao Tung University, Hsinchu 300, Taiwan, R.O.C. (phone: +886-3-5712121-54363; fax: +886-3-5715998; e-mail: dcliaw@cc.nctu.edu.tw).

Wen-Ching Chung, Ph.D. Candidate, Department of Electrical and Control Engineering, National Chiao Tung University, Hsinchu 300, Taiwan, R.O.C.

v : the longitudinal velocity.

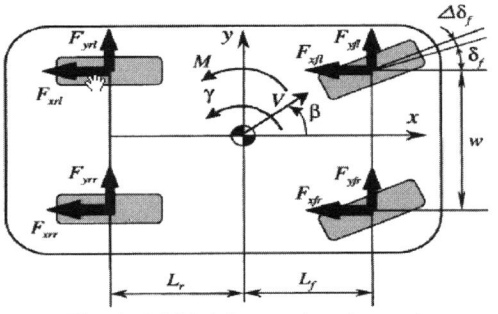

Fig. 1. Vehicle's steering dynamics.

In this study, we focus on the characteristic analysis of lateral dynamics by assuming $F_{xf} = 0$ and there are no acceleration or deceleration on the vehicle along longitudinal direction, i.e., $\dot{v} = 0$. Thus, Eq. (1) can be neglected for analysis. The steering dynamics for constant speed v can then be reduced to a second-order model as given by

$$\begin{aligned}\dot{\beta} &= f_1(\beta,\gamma,\delta_f) \\ &= \frac{1}{mv}\{F_{yf} + F_{yr}\} - \gamma, \end{aligned} \tag{4}$$

$$\begin{aligned}\dot{\gamma} &= f_2(\beta,\gamma,\delta_f) \\ &= \frac{1}{I_z}\{L_f F_{yf} - L_r F_{yr}\}\cos\beta, \end{aligned} \tag{5}$$

where both F_{yf} and F_{yr} are known functions of β, γ and δ_f.

III. Stability Analysis

In this section, we adopt the second-order model as in Eqs. (4)-(5) to study the local stability for the vehicle's steering dynamics. Denote $x^0 = (\beta^0, \gamma^0)^T$ an equilibrium point of system (4)-(5) for a given steering wheel angle $\delta_f = \delta_f{}^0$. By the definition of equilibrium point, we then have

$$F_{yf}(\beta^0,\gamma^0,\delta_f{}^0) + F_{yr}(\beta^0,\gamma^0,\delta_f{}^0) = \gamma^0 mv \tag{6}$$

and $$L_f F_{yf}(\beta^0,\gamma^0,\delta_f{}^0) - L_r F_{yr}(\beta^0,\gamma^0,\delta_f{}^0) = 0 \tag{7}$$

or $$\cos\beta^0 = 0. \tag{8}$$

To check the condition of Eq. (8), we have $\beta^0 = n\pi + \pi/2$ for n=0, 1, 2,… It is clear that a vehicle can not easily achieve such a condition. Thus, the equilibrium point x^0 in general should satisfy the conditions of Eqs. (6) and (7).

Let $x=(\beta,\gamma)^T$, $\tilde{x} = x - x^0$ and control input $u = \delta_f - \delta_f{}^0$. Taking the linearization of system (4)-(5) at x^0 and $\delta_f = \delta_f{}^0$, we have

$$\dot{\tilde{x}} = A\tilde{x} + Bu, \tag{9}$$

where

$$A = \begin{bmatrix} a_1 & a_2 \\ a_3 & a_4 \end{bmatrix} \quad \text{and} \quad B = \begin{bmatrix} b_1 \\ b_2 \end{bmatrix} \tag{10}$$

with

$$a_1 = \frac{1}{mv}\left(\frac{\partial F_{yf}}{\partial\beta} + \frac{\partial F_{yr}}{\partial\beta}\right)(\beta^0,\gamma^0,\delta_f{}^0), \tag{11}$$

$$a_2 = \frac{1}{mv}\frac{\partial}{\partial\gamma}\left(\frac{\partial F_{yf}}{\partial\gamma} + \frac{\partial F_{yr}}{\partial\gamma}\right)(\beta^0,\gamma^0,\delta_f{}^0) - 1, \tag{12}$$

$$a_3 = \frac{1}{I_z}\left(L_f\frac{\partial F_{yf}}{\partial\beta} - L_r\frac{\partial F_{yr}}{\partial\beta}\right)(\beta^0,\gamma^0,\delta_f{}^0)\cdot\cos\beta^0, \tag{13}$$

$$a_4 = \frac{1}{I_z}\left(L_f\frac{\partial F_{yf}}{\partial\gamma} - L_r\frac{\partial F_{yr}}{\partial\gamma}\right)(\beta^0,\gamma^0,\delta_f{}^0)\cdot\cos\beta^0, \tag{14}$$

$$b_1 = \frac{1}{mv}\left(\frac{\partial F_{yf}}{\partial\delta_f} + \frac{\partial F_{yr}}{\partial\delta_f}\right)(\beta^0,\gamma^0,\delta_f{}^0), \tag{15}$$

and $$b_2 = \frac{\cos\beta^0}{I_z}\left(L_f\frac{\partial F_{yf}}{\partial\delta_f} - L_r\frac{\partial F_{yr}}{\partial\delta_f}\right)(\beta^0,\gamma^0,\delta_f{}^0). \tag{16}$$

By applying the Routh-Hurwitz stability criterion, we then have the following stability result.

Lemma 1. The equilibrium point x^0 of system (4)-(5) is asymptotically stable if $a_1 + a_4 < 0$ and $a_1 a_4 - a_2 a_3 > 0$, where a_i's are given in Eqs. (11)-(14).

It is known from the so-called "Magic formula" (e.g., [5]-[6]) that both values of a_1 and a_4, in general, will be negative. Therefore, the stability condition of $a_1 + a_4 < 0$ is always satisfied. An example of a_i's will be given in Section V. Thus, the stability condition in Lemma 1 can then be reduced to that the equilibrium point x^0 of system (4)-(5) will be stable if $a_1 a_4 - a_2 a_3 > 0$. It is clear from $a_1 + a_4 < 0$ that the linearization system (4)-(5) at x^0 will not have a pair of pure imaginary eigenvalues with respect to the variation of β. Instead, the system dynamics might have one zero eigenvalue. This implies that the lateral dynamics of vehicle system will not undergo Hopf bifurcation but might have chance for the appearance of stationary bifurcation at some $\delta_f = \delta_f{}^0$ such that $a_1 a_4 - a_2 a_3 = 0$.

The conditions of the appearance of saddle node bifurcation for system (4)-(5) have been obtained in [12] as follows.

Lemma 2. The system (4)-(5) will undergo saddle node bifurcation for the equilibrium point x^0 if the following conditions hold:

(i) $a_1 a_4 = a_2 a_3$ with $a_1 < 0$ and $a_4 < 0$, (17)

(ii) $a_4 b_1 \neq a_2 b_2$, and (18)

(iii) $$a_4 q_{11} - a_3 q_{12} + \frac{a_3^2}{a_4} q_{13} - a_2 q_{21} + a_1 q_{22} - \frac{a_1^2}{a_2} q_{23} \neq 0, \tag{19}$$

where $q_{11}=\frac{\partial^2 f_1}{\partial^2 \beta}\left(x^0,\delta_f{}^0\right)$, $q_{12}=\frac{\partial^2 f_1}{\partial r\partial \beta}\left(x^0,\delta_f{}^0\right)$,

$q_{13}=\frac{\partial^2 f_1}{\partial^2 r}\left(x^0,\delta_f{}^0\right)$, $q_{21}=\frac{\partial^2 f_2}{\partial^2 \beta}\left(x^0,\delta_f{}^0\right)$,

$q_{22}=\frac{\partial^2 f_2}{\partial r\partial \beta}\left(x^0,\delta_f{}^0\right)$ and $q_{23}=\frac{\partial^2 f_2}{\partial^2 r}\left(x^0,\delta_f{}^0\right)$.

IV. Design of Stabilization Control Laws

As given in Lemma 2 above, system (4)-(5) could undergo stationary saddle node bifurcation, which might result in spin of vehicle. In order to prevent the appearance of such an instability, in this section we will seek for possible control laws for system stabilization. First, we will discuss the controllability of system (4)-(5). It is followed by the design of control laws for preventing and/or delaying the appearance of saddle node bifurcation. Details are given as follows.

A. Controllability Analysis

First, we check the controllability of system (4)-(5). Denote C the controllability matrix of the linearized model of system (4)-(5) as given in (9). We then have

$$C=\begin{bmatrix}B & AB\end{bmatrix} \tag{20}$$

$$=\begin{bmatrix}b_1 & a_1b_1+a_2b_2\\ b_2 & a_3b_1+a_4b_2\end{bmatrix}. \tag{21}$$

The determinant of the controllability matrix C is calculated as

$$\det[C]=a_3b_1^2-a_2b_2^2+\left(a_4-a_1\right)b_1b_2. \tag{22}$$

We have the next result.

Lemma 3. The linearized model (9) is controllable at the equilibrium point x^0 if $a_3b_1^2-a_2b_2^2+\left(a_4-a_1\right)b_1b_2\neq 0$, where a_i's and b_i's are given in Eqs. (11)-(16).

Next, we study a special case of which x^0 is the saddle node bifurcation point. From [12] and Lemma 2 in Section III, we have $a_1a_4-a_2a_3=0$ and $a_4b_1\neq a_2b_2$ when the linearized model is evaluated at the saddle node bifurcation point. Eq. (22) can then be rewritten as

$$\det\left[C\right]=\frac{1}{a_2}\left(a_4b_1-a_2b_2\right)\left(a_1b_1+a_2b_2\right). \tag{23}$$

The next result follows readily from Lemma 3.

Corollary 1. The stationary saddle node bifurcation point x^0 of system (4)-(5) is controllable if $a_1b_1+a_2b_2\neq 0$, where a_i's and b_i's are given in Eqs. (11)-(16).

B. State Feedback Control Design

As discussed above, the saddle node bifurcation point of system (4)-(5) is controllable if $a_1b_1+a_2b_2\neq 0$. This leads to the possibility of a design of state feedback control law for system stabilization. Let the control input $u=K\cdot\tilde{x}$, where $K=\begin{bmatrix}-k_1 & -k_2\end{bmatrix}$. The linearized model (9) can then rewritten as

$$\dot{\tilde{x}}=(A+BK)\cdot\tilde{x}. \tag{24}$$

The characteristic equation of system (24) gives

$$\lambda^2+h_1\lambda+h_2=0, \tag{25}$$

where

$$h_1=k_1b_1+k_2b_2-a_1-a_4, \tag{26}$$

and $$h_2=a_1a_4-a_2a_3+\left(a_2b_2-a_4b_1\right)k_1+\left(a_3b_1-a_1b_2\right)k_2. \tag{27}$$

By applying the Routh-Hurwitz stability criterion, we then have the following stabilization result for the equilibrium point x^0.

Theorem 1. The equilibrium point x^0 of system (4)-(5) is asymptotically stabilizable if $h_1>0$ and $h_2>0$, where h_1 and h_2 are given in Eqs. (26) and (27), respectively.

V. Case Study

It is known that there are many mathematical models have been proposed for cornering forces. In this paper, we adopt the so-called "Magic formula" from [6] for the models of nonlinear cornering forces F_{yf} and F_{yr}, respectively, as given by

$$F_{yf}=D_f\sin\left[C_f\tan^{-1}\left\{B_f(1-E_f)\alpha_f+E_f\tan^{-1}\left(B_f\alpha_f\right)\right\}\right] \tag{28}$$

and

$$F_{yr}=D_r\sin\left[C_r\tan^{-1}\left\{B_r(1-E_r)\alpha_r+E_r\tan^{-1}\left(B_r\alpha_r\right)\right\}\right], \tag{29}$$

where

$$\alpha_f=\beta+\tan^{-1}\left(\frac{L_f}{v}\gamma\cdot\cos\beta\right)-\delta_f \tag{30}$$

and $$\alpha_r=\beta-\tan^{-1}\left(\frac{L_r}{v}\gamma\cdot\cos\beta\right). \tag{31}$$

Here, B_i, C_i, D_i and E_i for $i = f, r$ are constants. α_f and α_r denote the slip angle of front tire and rear tire, respectively. It is clear from Eqs. (28) and (29) that $(\beta,\gamma)^T=(0,0)^T$ will make $F_{yf}=F_{yr}=0$ when $\delta_f=0$. Thus, $x^0=(0,0)^T$ is an equilibrium point for system (4)-(5) for $\delta_f=0$. This agrees with the natural behavior of vehicle dynamics.

In the following, we provide a case study for the lateral dynamics of vehicle system as given in system (4)-(5). To adopt the data from [5], we choose m = 1500 kg, I_z = 3000 kg·m^2, L_f = 1.2 m, L_r = 1.3m and v = 10-40 m/s. The values of remaining system parameters are chosen as given in Table I. In this study, the system parameters are chosen to be running on the low friction roads so that the vehicle might be easier to go into spin. This also corresponds to the driving condition of

traveling on a down sloping road at constant velocity with equivalent braking effect at throttle being off [5].

TABLE I

Symbol	High friction road	Low friction road
B_f, B_r	6.7651, 9.0051	11.275, 18.631
C_f, C_r	1.3, 1.3	1.56, 1.56
D_f, D_r	-6436.8, -5430	-2574.7, -1749.7
E_f, E_r	-1.999, -1.7908	-1.999, -1.7908

In this paper, the computer code AUTO [13] is used to do the numerical analysis, which can calculate system eigenvalues of Jacobian matrix at each equilibrium point and determine the corresponding system stability. Bifurcation diagram of system (4)-(5) with respect to the variation of δ_f is obtained as shown in Fig. 2. Note that, in the bifurcation diagram shown in this paper, the square box denotes the saddle node bifurcation point, the solid-line denotes the stable equilibrium point and the dashed-line denotes unstable equilibrium point, respectively. As shown in Fig. 2, all the system equilibrium points near the origin are found to be asymptotically stable for different setting value of the driving speed v, which were bounded by the saddle node bifurcation points. Location of those bifurcation points for different setting value of the driving speed v are listed in Table II. It is also observed from Fig. 2 that the system equilibrium changes stability at the saddle node bifurcation point and the magnitude of δ_f corresponding to the saddle node bifurcation becomes smaller as the velocity v increases.

TABLE II

v (m/s)	Label	δ_f (rad)	β^0 (rad)	γ^0 (rad/s)
10	SNBP01	-0.0569	0.0120	-0.2275
	SNBP02	0.0569	-0.0120	0.2275
15	SNBP03	-0.0260	0.0241	-0.1428
	SNBP04	0.0260	-0.0241	0.1428
20	SNBP05	-0.0158	0.0267	-0.1017
	SNBP06	0.0158	-0.0267	0.1017
25	SNBP07	-0.0114	0.0272	-0.0781
	SNBP08	0.0114	-0.0272	0.0781
30	SNBP09	-0.0090	0.0272	-0.0631
	SNBP10	0.0090	-0.0272	0.0631
35	SNBP11	-0.0076	0.0270	-0.0528
	SNBP12	0.0076	-0.0270	0.0528
40	SNBP13	-0.0067	0.0267	-0.0454
	SNBP14	0.0067	-0.0267	0.0454

To demonstrate the effectiveness of the proposed designs in Section IV, we consider to construct the linear control laws for system stabilization at the two bifurcation points SNBP01 and SNBP13, respectively. Details are given as follows.

A. Control Design for the Equilibrium Point SNBP01

First, we consider to design state feedback controllers for the low speed driving at v = 10 m/s. To check the controllability of SNBP01, we have $\det[C] = 209.211 \neq 0$. Hence, SNBP01 is controllable. The next result follows readily from Theorem 1 for system stabilization design at the point SNBP01.

Corollary 2. The saddle node bifurcation point SNBP01 of system (4)-(5) is asymptotically stabilizable by the linear control law if the feedback gains k_1 and k_2 satisfy the following two conditions:

$$\text{(i) } k_2 > -0.2838, \tag{32}$$

$$\text{(ii) } -2.5276 - 5.9996k_2 < k_1 < 0.0056 + 2.9267k_2. \tag{33}$$

As depicted in Fig. 2, the front-wheel angle δ_f will affect the existence of equilibrium points. In order to seek for a better control gains for system stabilization, let k_1 be treated as another bifurcation parameter. A two-parameter analysis of saddle node bifurcation is obtained for $k_2 = 0.1$ as depicted in Fig. 3, which indicate the location of saddle node bifurcation points. The symbol "s" in Fig. 3 denotes the stable operating zone, while "u" denotes the unstable operating zone. It is observed from Fig. 3 that the number of saddle node bifurcation will be different as k_1 varies. In addition to those bifurcation scenarios shown in Fig. 3, there are two more saddle node bifurcation points for $32.8656 > k_1 > -0.99$ and four saddle node bifurcation points for $-1.2605 < k_1 < -0.99$. Moreover, there is no saddle node bifurcation point for $k_1 < -1.2605$.

Figure 4 presents four saddle node bifurcation points when $k_1 = -1.2$ and $k_2 = 0.1$, and Figure 5 shows the bifurcation diagram with respect to the different setting of k_1 at $k_2 = 0.1$. The observations from of Fig. 3 are verified by those shown in Figs. 4 and 5. For $k_2 = 0.1$, the equilibrium point SNBP01 of system (4)-(5) is asymptotically stable when $-3.1276 < k_1 < 0.2982$. From Fig. 6, we can observe the stability of SNBP01 at different value of k_1. We found that SNBP01 is a stable equilibrium point for $k_1 = -1.5, -0.5$ and 0 while SNBP01 is an unstable equilibrium point for $k_1 = 0.5$ and 0.9. Those agree with the results of Corollary 2.

B. Control Design for the Equilibrium Point SNBP13

Next, we construct the stabilization control laws for the system (4)-(5) at the saddle node bifurcation point SNBP13. As observed in Fig. 2(a), the stable region of δ_f is very small for v = 40 m/s. To check the controllability of SNBP13, we have $\det[C] = 264.339 \neq 0$. Hence, the linearized model at the point SNBP13 is controllable. Follow the same control scheme as proposed in Theorem 1, we have the next result.

Corollary 3. The saddle node bifurcation point SNBP13 of system (4)-(5) is asymptotically stabilizable by the linear control law if the feedback gains k_1 and k_2 satisfy the following two conditions:

$$\text{(i) } k_2 > -0.1306, \tag{34}$$

$$\text{(ii) } -3.2952 - 23.9914k_2 < k_1 < 0.0004 + 1.2481k_2. \tag{35}$$

Similarly, let k_2 = 0.1. A two-parameter bifurcation diagram of δ_f and k_1 is depicted in Fig. 7, which presents the location of saddle node bifurcation points. There are two saddle node bifurcation points for $0.5341 > k_1 > -1$. If $k_1 <$

-1.1625, there is no saddle node bifurcation point. For $-1.1625 < k_1 < -1$, there are four saddle node bifurcation points. Figure 8 shows four saddle node bifurcation points at v=40 m/s, k_1 = -1.1 and k_2 = 0.1, and Fig. 9 shows bifurcation diagram with respect to the different values of k_1 at k_2 = 0.1. When k_1 = 1, there is no saddle node bifurcation point and all equilibrium points of system (4)-(5) are unstable. At k_2 = 0.1, the equilibrium point SNBP13 of system (4)-(5) is asymptotically stable for $-5.6943 < k_1 < 0.1252$. The stability of system (4)-(5) at SNBP13 for different values of k_1 is shown in Fig. 10. Those agree with the result of Corollary 3.

VI. Conclusions

In this paper, we focused on the nonlinear study of the second-order model of vehicle's lateral dynamics. The stationary bifurcation phenomenon is predicted and observed in this system. A direct state feedback design was proposed to stabilize the system at the bifurcation point. The two-parameter bifurcation analysis with respect to the setting of control gains were also obtained, which can provide a guide for the selection of the applied control efforts for preventing and/or delaying the occurrence of system instabilities.

References

[1] J. Y. Wong, *Theory of Ground Vehicles*. John Wiley & Sons, Inc., 2001.

[2] J. Ackerman, J. Guldner, W. Sienel, R. Steinhauser, and V. I. Utkin, "Linear and nonlinear controller design for robust automatic steering," *IEEE Trans. Contr. Syst. Technol.*, Vol. 3, pp. 132-143, 1995.

[3] H. Peng, and M. Tomizuka, "Vehicle lateral control for highway automation," *Proc. 1990 American Control Conference*, San Diego, CA, May 23-25, 1990.

[4] H. Peng, T. Hessburg, M. Tomizuka, and W. Zhang, "A theoretical and experimental study on vehicle lateral control," *Proc. 1992 American Control Conference*, Chicago, IL, June 24-26, 1992.

[5] E. Ono, S. Hosoe, H. D. Tuan, and S. Doi, "Bifurcation in vehicle dynamics and robust front wheel steering control," *IEEE Trans. Control Systems Technology*, Vol. 6, No. 3, pp. 412-420, 1998.

[6] L. R. Ray, "Nonlinear state and tire force estimation for advanced vehicle control," *IEEE Trans. Control Systems Technology*, Vol. 3, No. 1, pp. 117-124, 1995.

[7] N. Kopell and L. N. Howard, *Bifurcations and trajectories joining critical points*, Advances in Mathematics, Vol. 18, pp. 306-358, 1975.

[8] E. H. Abed and J. H. Fu, "Local feedback stabilization and bifurcation control, II. Stationary bifurcation," *System and Control Letters*, Vol. 8, pp. 467-473, 1987.

[9] D.-C. Liaw and E. H. Abed, "Stabilization of tethered satellites during station-keeping," *IEEE Trans. Automatic Control*, Vol. 35, No. 11, pp. 1186-1196, 1990.

[10] D.-C. Liaw and E. H. Abed, "Active control of compressor stall inception: a bifurcation-theoretic approach," *Automatica*, Vol. 32, No. 1, pp. 109-115, 1996.

[11] D.-C. Liaw and C.-C. Song, "Analysis of longitudinal flight dynamics: a bifurcation-theoretic approach," *Journal of Guidance, Control, and Dynamics*, Vol. 24, No. 1, pp. 109-116, 2001..

[12] D.-C. Liaw, H.-H. Chiang, and T.-T. Lee, "A bifurcation study of vehicle's steering dynamics," *Proc. IEEE 2005 Intelligent Vehicles Symposium*, Las Vegas, Nevada, USA, June 6-8, 2005, pp. 388-393.

[13] E. J. Doedel, *AUTO: A program for the automatic bifurcation analysis of autonomous systems*. Congressus Numerantium, Vol. 30, pp. 265-284, 1981.

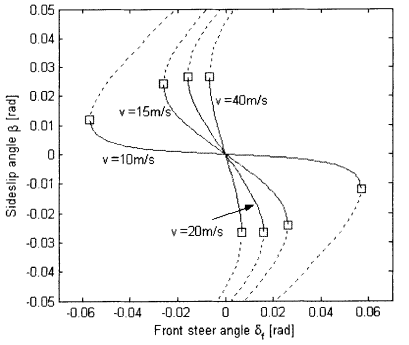

(a) δ_f v.s. β

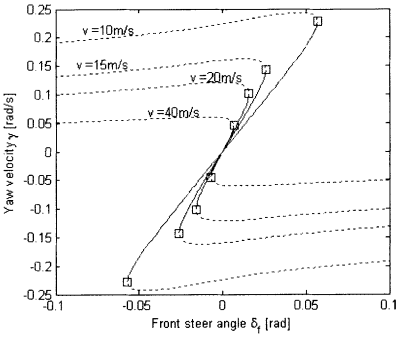

(b) δ_f v.s. γ

Fig. 2. Bifurcation diagram with respect to different v.

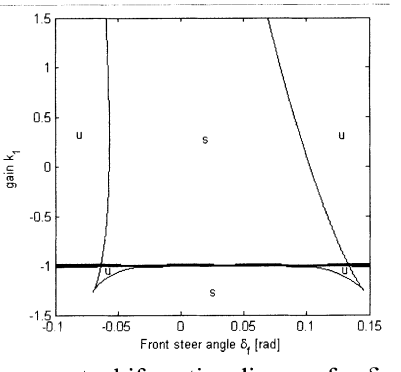

Fig. 3. Two-parameter bifurcation diagram for δ_f v.s. k_1 when v=10 m/s and k_2 = 0.1.

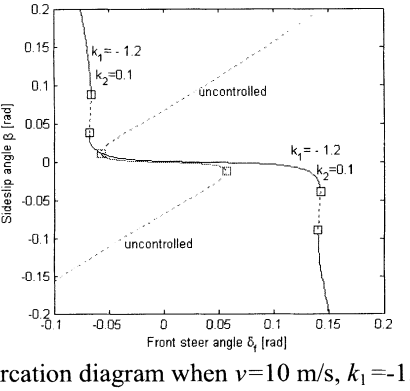

Fig. 4. Bifurcation diagram when v=10 m/s, k_1 =-1.2 and k_2 = 0.1.

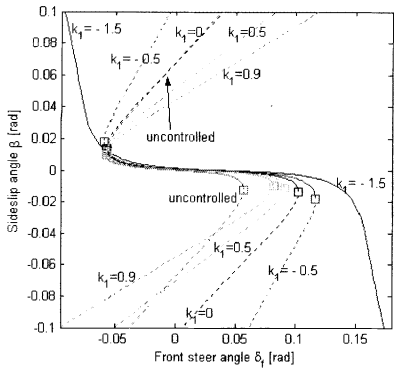

(a) δ_f v.s. β

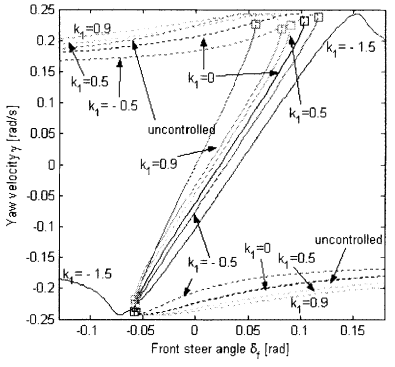

(b) δ_f v.s. γ

Fig. 5. Bifurcation diagram with respect to different k_1 when v=10 m/s and k_2 = 0.1.

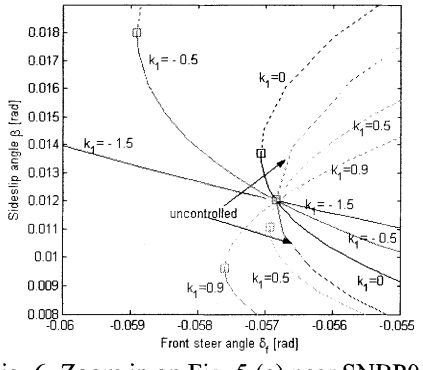

Fig. 6. Zoom in on Fig. 5 (a) near SNBP01.

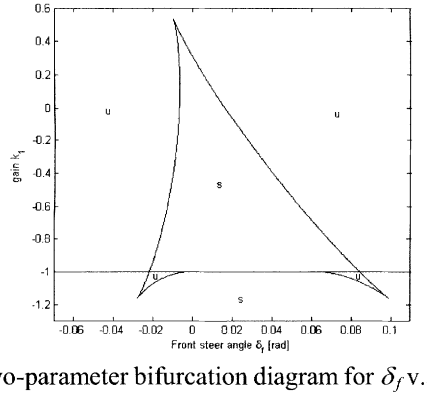

Fig. 7. Two-parameter bifurcation diagram for δ_f v.s. k_1 when v=40 m/s and k_2 = 0.1.

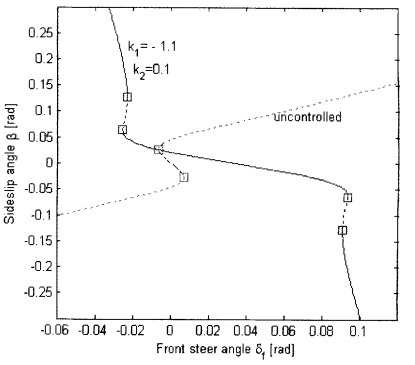

Fig. 8. Bifurcation diagram when v=40 m/s, k_1 =-1.1 and k_2 = 0.1.

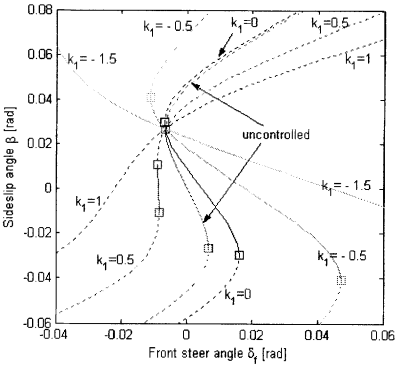

(a) δ_f v.s. β

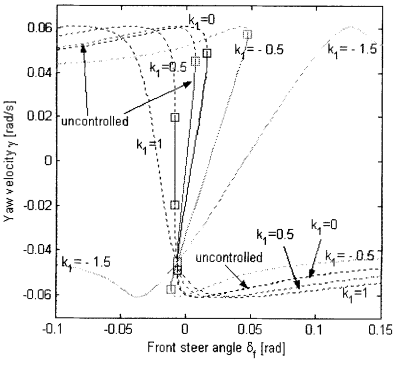

(b) δ_f v.s. γ

Fig.9. Bifurcation diagram with respect to different k_1 when v=40 m/s and k_2 = 0.1.

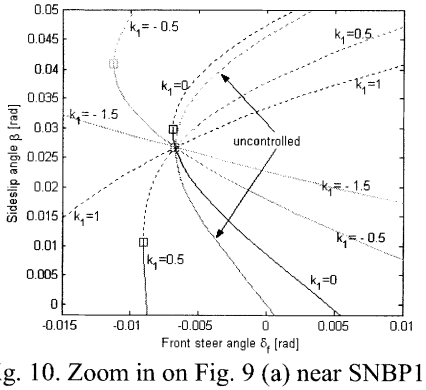

Fig. 10. Zoom in on Fig. 9 (a) near SNBP13.